

exothermicity is expected to be found as vibrational excitation energy. Taking into account the excitation up to $v = 7$, Bourguignon et al.²¹ determined a lower limit for $\langle f_{\text{vib}} \rangle$ of 0.18 while the fraction stored into rotational excitation (f_{rot}) amounts at least to 0.22. This contrasts with the $\text{Ca}(^1\text{S}) + \text{Cl}_2$ reaction where 70% of the reaction energy goes to vibrational excitation of the CaCl molecule.²⁴ In view of the presence of an energy barrier of $3.6 \pm 0.3 \text{ kJ mol}^{-1}$ and the energy distribution in the MgCl product molecule which is quite different from that in CaCl , the original concept of "harpooning" might not be applicable to reaction 3. A more appropriate terminology would be a "close-range" charge-transfer mechanism.

Concerning the possibility of a second electron transfer it has been pointed out by Bourguignon et al.^{8a} that the distance to form the double ionic species lies at 2.3 \AA which is in the range of the r_c values derived in this work. In this respect a distinction between a single and double electron-transfer model would be meaningless. However, in analogy with $\text{Ca}(^1\text{S}) + \text{Cl}_2$, the reaction to form $\text{Mg}^{2+} + \text{Cl}^{2-}$ should proceed according to C_{2v} symmetry path. In that case the reaction shows a barrier at the entrance channel so that the occurrence of a second electron transfer becomes less probable.

In conclusion, it can be stated that, from the magnitude of the rate constant k_3 of the $\text{Mg}(^1\text{S}) + \text{Cl}_2$ reaction, direct experimental proof is obtained for a "close-range" interaction involving a charge transfer at distances of less than 3 \AA . Measurements are now under way to determine the rate constant of the $\text{Cu}(^2\text{S}) + \text{Cl}_2$ reaction. With an ionization energy of copper of 7.72 eV close to the value of 7.64 eV for magnesium atoms, it will be interesting to see whether this mechanism can also be extended to transition metal/halogen reactions.

Acknowledgment. We thank the Fund for Joint Basic Research (FKFO), Belgium, for a research grant. C.V. is a Research Director of the National Fund for Scientific Research (Belgium). P.C. is grateful to the Institute for Scientific Research in Agriculture and Industry for granting him a doctoral fellowship.

Registry No. Mg, 7439-95-4; Cl_2 , 7782-50-5.

References and Notes

- (1) Polanyi, M. *Atomic Reactions*; Williams and Norgate Ltd.: London, 1932.
- (2) Magee, J. J. *Chem. Phys.* **1940**, *8*, 687.
- (3) Herschbach, D. R. *Adv. Chem. Phys.* **1966**, *10*, 319.
- (4) Levy, M. R. *Prog. React. Kinet.* **1981**, *10*, 1.
- (5) Maya, J.; Davidovits, P. J. *Chem. Phys.* **1973**, *59*, 3143.
- (6) Maya, J.; Davidovits, P. J. *Chem. Phys.* **1974**, *61*, 1028.
- (7) Edelstein, S. A.; Davidovits, P. J. *Chem. Phys.* **1971**, *55*, 5164.
- (8) See also references in the following papers: (a) Bourguignon, B.; Gargoura, M. A.; Rostas, J.; Taieb, G. J. *Phys. Chem.* **1987**, *91*, 2080. (b) Menzinger, M. In *Gas-Phase Chemiluminescence and Chemi-ionization*; Fontijn, A., Ed.; Elsevier Science: New York, 1984; p 25.
- (9) Honjou, N.; Yarkony, D. R. *J. Phys. Chem.* **1985**, *89*, 2919.
- (10) Menzinger, M. *Adv. Chem. Phys.* **1980**, *42*, 1.
- (11) Kashireninov, O. E.; Manelis, G. B.; Repka, L. F. *Russ. J. Phys. Chem.* **1982**, *56*, 630.
- (12) Vinckier, C.; Dumoulin, A.; De Jaegere, S. J. *Chem. Soc., Faraday Trans. 2* **1988**, *84*, 1725.
- (13) Vinckier, C.; Christiaens, P.; Hendrickx, M. In *Gas Phase Metals Reactions*; Fontijn, A., Ed.; Elsevier: New York, in press.
- (14) Vinckier, C.; Christiaens, P. *J. Phys. Chem.* **1992**, *96*, 2146.
- (15) SAS statistical package, SAS Institute Inc., Cary, NC, 1989.
- (16) Talcott, C. L.; Ager III, J. W.; Howard, C. J. *J. Chem. Phys.* **1986**, *84*, 6161.
- (17) Fontijn, A.; Felder, W. *Reactive Intermediates in the Gas Phase, Generation and Monitoring*; Setser, D. W., Ed.; Academic Press: New York, 1979; p 59.
- (18) Baulch, D. L.; Duxbury, J.; Grant, S. J.; Mantague, D. C. *J. Phys. Chem. Ref. Data* **1981**, *10*, Suppl. 1, 1-1.
- (19) Lin, S. M.; Mims, C. A.; Herm, R. R. *J. Chem. Phys.* **1973**, *58*, 327.
- (20) Jonah, C. D.; Zare, R. N. *Chem. Phys. Lett.* **1971**, *9*, 65.
- (21) Shafizadeh, N.; Rostas, J.; Taieb, G.; Bourguignon, B. *Chem. Phys.* **1990**, *142*, 111.
- (22) Rostas, J.; Shafizadeh, N.; Taieb, G.; Bourguignon, B. *Chem. Phys.* **1990**, *142*, 97.
- (23) Huber, K. P.; Herzberg, G. *Molecular Spectra and Molecular Structure IV: Constants of Diatomic Molecules*; Van Nostrand: New York, 1979.
- (24) Dagdigian, P. J. In *Gas Phase Chemiluminescence and Chemi-ionization*; Fontijn, A., Ed.; North Holland: Amsterdam, 1985; p 203.

Kinetic Study of the $\text{OH} + \text{H}_2$ Reaction from 800 to 1550 K

R. C. Oldenberg,* G. W. Loge, D. M. Harradine, and K. R. Winn

Chemical and Laser Sciences Division, Los Alamos National Laboratory, Los Alamos, New Mexico 87545
(Received: May 22, 1992; In Final Form: July 7, 1992)

Direct measurements of the rate constant for the bimolecular reaction $\text{OH} + \text{H}_2 \rightarrow \text{H} + \text{H}_2\text{O}$ have been completed in the temperature range 800–1550 K. In these experiments, small amounts of water vapor were photolyzed with an excimer laser to "instantaneously" create OH radicals and H atoms. The subsequent time history of the OH radicals was monitored by using laser-induced fluorescence. Analysis of the OH removal rate as a function of added hydrogen yielded the rate constant for the above reaction. The temperature range of our measurements bridges the gap between the recent shock tube data (1246–2581 K) of Michael and Sutherland; Frank and Just; Davidson, Chang, and Hanson and the quartz cell flash photolysis data (250–1050 K) of Tully, Ravishankara, and co-workers. Our data are in very good agreement with these previous data sets in the overlap region. By combining our data with these four data sets, we derive a new rate constant expression, $k = (3.56 \times 10^{-16})T^{1.52} \exp[-1736/T] \text{ cm}^3 \text{ molecule}^{-1} \text{ s}^{-1}$, that is applicable in the temperature range 250–2581 K.

Introduction

The bimolecular reaction of hydroxyl radicals with molecular hydrogen

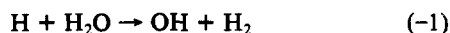


is a critical chain-propagating reaction in hydrogen combustion and, together with the reverse reaction, contributes significantly to the establishment of partial equilibrium in postcombustion gases. This reaction is also the main source of water in typical hydrocarbon/air flames at atmospheric pressure. Because of its im-

portance in combustion, this reaction has been the subject of numerous indirect measurements and critical reviews.¹ This reaction is also of more fundamental interest because of the distinct non-Arrhenius behavior of its rate constant, consistent with many atomic hydrogen abstraction reactions involving the OH radical.²

The rate constant for this reaction was reinvestigated by Tully, Ravishankara, and co-workers using a flash photolysis/resonance fluorescence technique in a heated quartz cell.^{3,4} Their data spanned the temperature range from 250 to 1050 K and clearly demonstrated the non-Arrhenius behavior of the reaction in a

single experiment. Frank and Just⁵ used a shock tube/resonance fluorescence technique to study reaction 1 in the range 1693–2574 K. While the data in this temperature range could be represented in a simple Arrhenius form, it was fairly consistent with the curvature shown previously. Recently, Michael and Sutherland⁶ studied the reverse of reaction 1, namely



in the temperature range 1246–2297 K using a flash photolysis/shock tube technique. Using their shock tube data and the JANAF thermochemical tables to calculate equilibrium constant for the reverse reaction,⁷ they calculated a temperature-dependent rate constant for reaction 1. They combined these values with those of Frank and Just and the flash photolysis data of Tully, Ravishankara, and co-workers and derived the expression

$$k_1 = (3.59 \times 10^{-16})T^{1.51} \exp[-1726/T] \text{ cm}^3 \text{ molecule}^{-1} \text{ s}^{-1} \quad (\text{I})$$

which is applicable in the temperature range 250–2581 K. Davidson et al.⁸ used a laser photolysis/shock tube technique to measure the rate of reaction -1 by monitoring the production of the OH radical with dye laser absorption. Using these data, they derived rate constants for reaction 1 in the temperature range 1647–2493 K that are slightly higher than predicted by the Michael and Sutherland expression noted above.

We report here direct measurements of k_1 over the temperature range 800–1550 K using a laser photolysis/heated flow cell technique and using laser induced fluorescence to monitor the OH radicals. These new measurements bridge the gap between the shock tube data (1246–2581 K) and the quartz cell data (250–1050 K) and are in good agreement with these previous data sets in the overlap region, with a slightly smaller value in the higher temperature region than predicted by eq I. This new data set was combined with the data used to obtain eq I and the data of Davidson et al. to obtain a new expression. The new expression for the temperature dependence of the rate constant for reaction 1 has an improved statistical precision and accuracy resulting from more data taken by different techniques used in the fit.

Experimental Design

Our approach to measuring the temperature dependence of k_1 was to use a heated alumina ceramic tubular cell through which a premixed gas of H₂O in Ar was flowed along with H₂ reactant and Ar buffer gases. The H₂O was photolyzed by using an ArF excimer laser at 193 nm and the OH number density was monitored at various delay times after the photolysis pulse by using a pulsed Nd:YAG laser-pumped dye laser with gated detection of the OH fluorescence.

The details of the alumina ceramic cell construction have been given previously.⁹ Briefly, it consists of an inner alumina tube that is wrapped with Pt:Rh wire, which has a melting point of 1920 K and is oxidation resistant. The ceramic tube has two sets of holes in the sides, one to allow the photolysis and probe laser beams through and one to allow fluorescence collection. This wire-wrapped cell is surrounded with Zircar insulation and is contained in a water-cooled brass can with windows on the sides for the laser beams and fluorescence collection. The windows were purged by using an argon flow of 25 sccm that filled the volume between the outer cooled can and the inner ceramic cell and flowed into the cell after purging the windows.

The temperature inside the cell was regulated by using Pt sheathed, Pt:Rh thermocouples located several centimeters above and below the laser photolysis/LIF region that were in a feedback circuit with the heater wires at the top and bottom of the cell. These thermocouples did not give an accurate measure of the gas temperature in the laser photolysis/LIF viewing zone. Rather, to measure the gas temperature in this zone, a movable, Pt-sheathed, Pt:Rh thermocouple was lowered into place to accurately measure the temperature and then retracted during laser photolysis/LIF data acquisition. By moving the thermocouple up or down in 1-mm increments, a rough estimate of the temperature gradient of the gas in the region of the laser photolysis/LIF zone

was found to be about 2 deg/mm.

The accuracy of this thermocouple reading was checked by comparing it to a rotational temperature of the OH radicals produced by photolysis of H₂O. This was measured by using observed rotational LIF line intensities and known OH rotational line strengths.^{10,11} It was found that double-thermal shields¹² were needed to prevent radiative coupling of the thermocouple with the holes in the cell, which would have otherwise given a low reading for the gas temperature in the observation region. Once properly shielded the thermocouple readings were estimated to have an accuracy of $\pm 2^\circ$ and were far more precise than the LIF rotational temperature measurements. The temperature was regulated by using the heater feedback thermocouples to $\pm 1^\circ$.

A premixed gas was used to introduce the H₂O into the cell, which consisted of 1% H₂O vapor in Ar that was allowed to mix for several days in a large tank (approximately 20 L) before using. This mixture was flowed into a final mixing manifold, where it was allowed to mix with the H₂ reactant and Ar diluent gases, and then flowed into the cell where it was heated before reaching the laser photolysis region. The total pressure in the cell was controlled to 200 Torr by using a needle valve between the cell and the vacuum pump. The partial pressures of the gases were controlled by using flow metering valves. The 1% H₂O in Ar mix was flowed at a rate of 10 sccm, while the Ar diluent gas was flowed at 500 sccm, which along with the 25 sccm flow rate of the window purge gas gave a total flow rate of 535 sccm and a H₂O partial pressure of 37 mTorr. The only exceptions to this were three data sets taken at the lowest temperatures, where the 1% H₂O in Ar mix was flowed at 100 sccm to give a higher H₂O partial pressure to offset the reduced photolysis cross-section used to produce the OH radicals. The H₂ reactant gas was also metered into the manifold by using a 10-sccm flow-controlled valve at various rates to allow the OH removal rate to be measured for various H₂ partial pressures. The flow metering values used for all the gases were calibrated for the gas used by measuring the rate of pressure rise in a known collection volume.

The ArF excimer laser used was equipped with unstable resonator optics and was focused by using a cylindrical lens with a spherical lens to give a 3 mm \times 3 mm spot at the focus in the center of the cell. This was checked by using a beam splitter located immediately in front of the cell window to allow viewing the focus outside the cell with a diode array. Typically 2–5 mJ of energy entered the cell.

The dye laser beam was made collinear with the photolysis laser beam by using a dichroic mirror that transmitted near-UV and reflected 193 nm. It was focused by using a spherical lens to give a spot size of 1 mm and was centered on the excimer beam to reduce the effects of OH diffusion out of the LIF beam so the OH removal rate would be dominated by reaction with H₂. The overlap of the two beams was checked by using the beam splitter and diode array setup.

The dye laser wavelength was tuned to the 0–0 vibrational band of the OH $^1\Sigma^+ \rightarrow ^1\Pi$ transition in the region 308–312 nm. For the OH decay time profiles the wavelength was tuned to the P₂(5) rotational line at 310.85 nm, which was one of the stronger fully resolved lines in the temperature range used.¹¹ In most experiments the dye laser had sufficient fluence to partially saturate the stronger OH rotational absorption lines, which was checked by using ND filters in the beam and observing the LIF line intensity. For typical laser powers used, the stronger rotational lines of the OH absorption were seen to be saturated both by smaller peak heights relative to the weaker lines and by a broadening of the laser linewidth of 0.5 cm⁻¹ to observed linewidths of about 0.7 cm⁻¹. For the decay histories this was not a problem and actually helped to reduce noise due to laser fluctuations. However, to measure gas temperatures using rotational line intensities, saturation had to be completely avoided. This was done by using an attenuator of ND = 1.0 in the dye laser beam.

The LIF was collected with a 10-cm focal length lens and filtered by using a 0.25-m monochromator with 2-mm slits at 307 nm with a bandwidth of 3.3 nm to discriminate against scattered laser light. Rotational relaxation of the ground-state OH formed

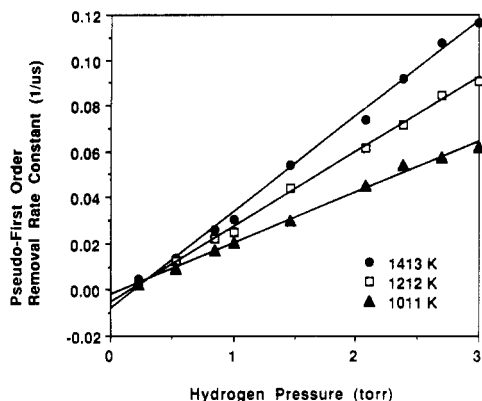


Figure 1. Pseudo-first-order OH decay rate, obtained as a linear regression fit to the logarithm of the OH signal as a function of the delay time after formation by photolysis, is plotted as a function of the H_2 partial pressure. Only a few representative temperatures are shown. The results for all temperatures are listed in Table I. The error bars are smaller than the symbols. The straight line is the linear regression fit.

by photolysis was accomplished by using about 200 Torr of Ar buffer gas. Emission from the excited state OH was also determined to be rotationally relaxed within the fluorescence lifetime by scanning the 0.25-m monochromator.

The fluorescence was detected by using a PMT and was converted to a voltage signal by using a preamp. This was put into a boxcar averager that was triggered at the same time as the dye laser. The gate width used was 200 ns and was delayed 200 ns after the dye laser pulse to reduce scattered laser light. The boxcar was used in the linear averaging mode. Typically ten pulses were taken at each delay time with the LIF signal averaged, then the boxcar was cleared by the computer.

To obtain decay histories of OH, the dye laser pulse and boxcar gates were delayed by a variable time after the excimer laser pulse with a computer-controlled delay generator. Ten percent of the delay time scale included a negative delay time to allow determination of the baseline signal due to scattered dye laser light before the excimer laser formed OH. The delay time between the photolysis laser and the probe laser pulses was varied randomly to avoid systematic errors. This was repeated until the entire OH decay history was obtained with less than 10% difference in LIF amplitude between adjacent acquired data points.

Results and Discussion

The OH decay profiles were fit to an exponential decay by taking the logarithm of the LIF signal, assuming pseudo-first-order rate constant conditions from an excess of H_2 . Before taking the logarithm of the OH LIF signal as a function of delay time, the baseline signal was subtracted. The logarithm of the baseline-corrected LIF signal vs time was then fit by using a linear regression. All of the results fit the exponential decay to greater than three lifetimes. The slope of the regression gave the pseudo-first-order rate constant for a constant H_2 pressure. The pseudo-first-order rate constant was obtained for several H_2 pressures and plotted as a function of H_2 pressure to allow determination of the rate constant k_1 from the slope of the plot by using a second linear regression analysis. A typical plot for three representative temperatures is illustrated in Figure 1. This procedure was then repeated for several temperatures to obtain the rate constant as a function of temperature. The results are presented in Table I with one standard deviation of the fit.

It can be seen from Table I and Figure 1 that nearly all the fits have negative intercepts, which tend to get more noticeable at higher temperature. This is most likely due to population in the higher vibrational levels of ground-state OH formed by photolysis being relaxed to the lowest vibrational level, which is the only level probed by LIF.

A kinetic model that includes vibrational level relaxation of OH to the zero vibrational level as well as reaction with H_2 was used to determine its effect on the OH removal rate as a function of H_2 partial pressure. vibrationally excited OH has been shown

TABLE I^a

temp, K	rate constant, $10^{12} \text{ cm}^3 \text{ s}^{-1}$	intercept, 10^{-3} s^{-1}
809	1.068 ± 0.027	-1.2 ± 0.6
858	1.335 ± 0.058	0.2 ± 1.4
908	1.640 ± 0.029	-1.4 ± 0.7
977	2.143 ± 0.107	-0.5 ± 2.2
1011	2.326 ± 0.063	-1.9 ± 1.1
1077	3.020 ± 0.066	-1.7 ± 1.1
1080	3.055 ± 0.122	-1.2 ± 2.2
1086	3.162 ± 0.082	-4.0 ± 1.3
1111	3.131 ± 0.035	-3.5 ± 0.6
1181	4.166 ± 0.155	-1.3 ± 2.5
1212	4.080 ± 0.078	-5.2 ± 1.1
1213	4.249 ± 0.244	-2.7 ± 3.9
1281	5.159 ± 0.132	-1.4 ± 2.0
1282	5.104 ± 0.166	-1.8 ± 2.6
1312	4.952 ± 0.120	-8.2 ± 1.6
1343	5.767 ± 0.102	-3.8 ± 1.4
1397	6.487 ± 0.097	-7.0 ± 1.2
1413	6.110 ± 0.148	-8.3 ± 1.9
1513	7.261 ± 0.238	-7.5 ± 3.0
1548	7.875 ± 0.608	-11.3 ± 6.6

^a All of the rate constants obtained at various temperatures are listed with one standard deviation of the linear regression fit and the intercept of the fit.

to react with H_2 at nearly the same rate as zero vibrational level OH,¹³ which simplifies the kinetic model. Using this model, the rate of exchange of vibrationally excited and ground-state OH can be written as

$$d[\text{OH}]^*/dt = -k_1[\text{H}_2][\text{OH}]^* - k_{vr}[\text{M}][\text{OH}]^* \quad (\text{II})$$

$$d[\text{OH}]/dt = -k_1[\text{H}_2][\text{OH}] + k_{vr}[\text{M}][\text{OH}]^* \quad (\text{III})$$

where $[\text{OH}]^*$ is vibrationally excited OH and k_{vr} is the rate constant for vibrational relaxation by collision with a partner, M. In this simplified treatment all the OH in vibrationally excited states is grouped together as OH^* . Clearly, a more comprehensive model would treat each excited vibrational state separately, each with a distinct relaxation rate constant. However, the limited scope of the data presented here does not justify this additional complexity.

Solution of eqs II and III for $[\text{OH}]$ by integration, assuming constant $[\text{H}_2]$, gives $[\text{OH}] = \{[\text{OH}]_0 + [\text{OH}]_i^*\} \exp(-k_1[\text{H}_2]t)$, where $[\text{OH}]_i^* = [\text{OH}]_0^* [1 - \exp(-k_{vr}[\text{M}]t)]$. When the natural logarithms of $[\text{OH}]$ is plotted as a function of time, the predicted slope is

$$-d(\ln [\text{OH}])/dt = k_1[\text{H}_2] - k_{vr}[\text{M}] \{ [\text{OH}]_0^* - [\text{OH}]_i^* \} / \{ [\text{OH}]_0 + [\text{OH}]_i^* \} \quad (\text{IV})$$

where $-d(\ln [\text{OH}])/dt$ is the pseudo-first-order rate constant. Since the actual plots of the natural logarithm of $[\text{OH}]$ as a function of time are linear to greater than three lifetimes, one of two limiting cases of the vibrational relaxation rate must be occurring. For slow vibrational relaxation ($k_{vr}[\text{M}]t \ll 1$), eq IV becomes

$$-d(\ln [\text{OH}])/dt = k_1[\text{H}_2] - k_{vr}[\text{M}][\text{OH}]_0^* / [\text{OH}]_0 \quad (\text{V})$$

For fast vibrational relaxation ($k_{vr}[\text{M}] \gg 1$), eq IV becomes

$$-d(\ln [\text{OH}])/dt = k_1[\text{H}_2] \quad (\text{VI})$$

In both cases the slope is predicted to be a linear function of $[\text{H}_2]$, giving $k_1[\text{H}_2]$ unambiguously, but eq V also predicts a nonzero value when $[\text{H}_2]$ is zero. As can be seen from Figure 1, which plots the removal rate constant as a function of $[\text{H}_2]$, there is a negative intercept as predicted by eq V. For very low or zero pressures of H_2 , eq V also predicts that the observed removal rate constant would be negative, i.e., that the rate of OH formation through vibrational relaxation would exceed the rate of removal by reaction 1. Consistent with this prediction, the OH time histories under these conditions show a small exponential rise, followed at much longer times by a decay due to diffusion of OH out of the laser beam viewing zone. In principle, an analysis of the small exponential rise could be incorporated in our reaction rate determination. In practice, however, the rates obtained from

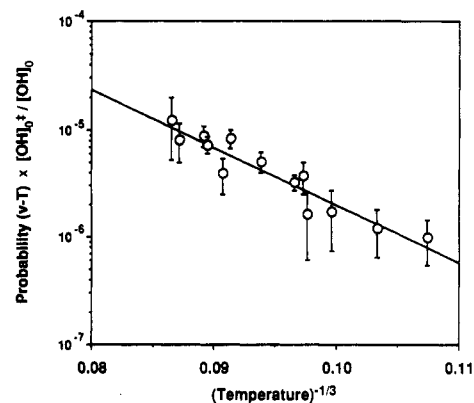


Figure 2. The intercepts of the data, as seen in Figure 1 and listed in Table I, are converted to the ratio of the rate of OH vibrational relaxation over the hard-sphere collision rate times the nascent ratio of vibrational excited OH to ground-state OH, assuming the kinetic model discussed in the text. The logarithm of these values is plotted as a function of the cube root of the temperature in a Landau-Teller plot. Points that had a standard deviation larger than their magnitude are omitted.

the rise were of much poorer precision. Consequently, only data at H₂ pressures for which the first term in equation V dominated the kinetics and well exceeded the latter vibrational relaxation term were used in the determination of the reaction rate constants, k_1 .

As can be seen in Table I, the observed intercept gets larger at higher temperature, within the experimental error. This is also consistent with eq V since the rate constant for vibrational relaxation, which is part of the intercept predicted by eq V, is expected to increase with temperature if the process does not involve an attractive (i.e., polar) intermolecular potential,¹⁴ which seems reasonable for OH-Ar collisions. This has been reported for the similar system of vibrational relaxation of $2\nu_2$ in H₂O by Ar.¹⁵ Also, the ratio of vibrationally excited OH to ground-state OH formed by photolysis most likely would increase slightly for higher temperatures of the parent H₂O molecule, because more vibrational energy would be available to the OH fragment. Thus, the observed trend of increasingly negative intercepts with increasing temperature is consistent with the slow vibrational relaxation mechanism.

Some attempts to obtain estimates for the vibrational relaxation rate constant and the nascent ratio of vibrationally excited OH to ground-state OH were made to ascertain that they were reasonable, giving a check on the validity of this model to explain the negative intercepts. This was done by assuming that $[\text{OH}]_0^*/[\text{OH}]_0 \leq 1$. Using this along with the observed intercept of the $-\text{d}(\ln[\text{OH}])/dt$ vs $[\text{H}_2]$ linear regression fits allows a lower limit for the vibrational relaxation rate constant to be obtained from the intercept, within the rather large uncertainty of the numbers. At 900 K this is about $>10^{-16}$ cm³/s. This is consistent with the previously reported upper limit of $<10^{-14}$ cm³/s for the vibrational relaxation rate constant of OH($\nu = 2$) by Ar at 300 K.^{16,17} Using a larger upper limit for $[\text{OH}]_0^*/[\text{OH}]_0$ would have given a smaller lower limit for the relaxation rate constant, but the value of $>10^{-16}$ cm³/s is consistent with the assumption of slow vibrational relaxation compared to the reaction rate.

As a second check on the validity of the vibrational model to explain the negative intercepts, the temperature dependence was compared to the expected temperature dependence for vibrational relaxation involving a nonattractive potential by using the simple Landau-Teller model. This was performed by assuming $[\text{OH}]_0^*/[\text{OH}]_0$ formed by photolysis of H₂O does not change with temperature. Therefore, the intercept divided by the hard-sphere collision rate is proportional to the probability of a hard-sphere collision causing vibrational relaxation. The logarithm of this quantity is plotted vs the inverse cube root of temperature in a Landau-Teller plot (Figure 2). This is expected to be a straight line for a nonattractive potential interaction and is within the error. The slope of Figure 2 is consistent with the expected temperature dependence for a repulsive potential of $V = V_0 \exp[-17(\text{\AA}^{-1})r]$,

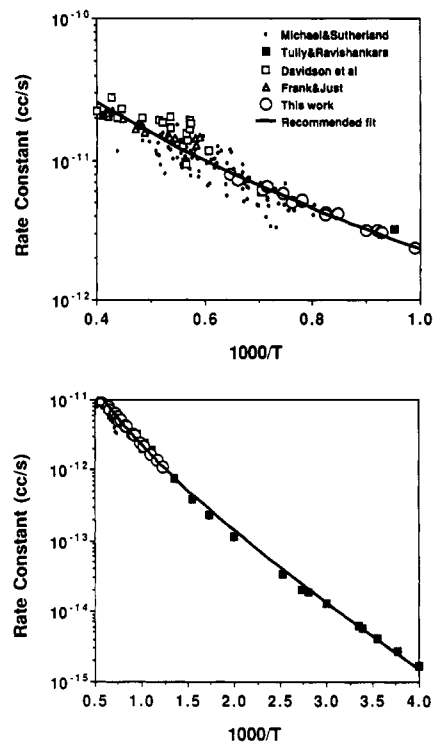


Figure 3. The weighted linear regression fit to the combined data sets is shown as the solid line. The data are shown in an Arrhenius plot that is broken into two temperature ranges to show better the data sets.

which is reasonable for an Ar-OH intermolecular potential.

If H₂ is causing any vibrational relaxation of OH, it would add to the $[\text{H}_2]$ dependence in eq V and give a larger slope to plots like Figure 1, making the slope larger than k_1 by $k_{\text{vr}}[\text{OH}]_0^*/[\text{OH}]_0$. This additional term should be several orders of magnitude less than k_1 if H₂ gives a relaxation rate comparable to that of Ar. Consequently, using the slope of plots like Figure 1 should not introduce any significant systematic error in k_1 obtained in this manner.

The rate constants obtained for k_1 in the temperature range 800–1550 K as listed in the table were combined with previous data to obtain an overall best expression for the temperature dependence of the rate constant from a linear least-squares fit to a modified Arrhenius expression. The rate constant measurements shown in the table are the result of typically nine measurements of the OH decay rate for different H₂ pressures (see Figure 1). Consequently, these data are included with the number of measurements as a weighting factor in the linear least-squares fit to the temperature dependence of the rate constant. The shock tube data of Michael and Sutherland; Frank and Just; and Davidson, Chang, and Hanson were included with a weighting of unity for the rate constant at each temperature because each data point represented the rate measurement for only one H₂ pressure. The quartz cell flash photolysis data (250–1050 K) of Tully, Ravishankara, and co-workers were included with a weighting factor six, taken as the number of measurements of the rate constant at each temperature for various amounts of H₂, as done in the present experiments. It should be noted, however, that because all the data are fairly consistent, the selection of weighting factors does not significantly alter the final expression.

The linear least-squares fit obtained by using this procedure is shown in Figure 3. The fitted expression is

$$k_1 = (3.56 \times 10^{-16}) T^{1.52} \exp[-1736/T] \text{ cm}^3 \text{ molecule}^{-1} \text{ s}^{-1} \quad (\text{VII})$$

and is applicable in the temperature range 250–2581 K. This expression is remarkably similar to the expression in eq I obtained by Michael and Sutherland. It should be noted that the new expression would not have been so similar to the previous one if the data of Davidson et al. had not been included. The rate

